ELSEVIER

Contents lists available at ScienceDirect

Computational Materials Science

journal homepage: www.elsevier.com/locate/commatsci



Full Length Article



The mechanism of adsorptive desulfurization on Cu and Ce exchanged Y zeolite using density functional theory

Henry J. Sokol, Kevin X. Lee, Julia A. Valla

Department of Chemical and Biomolecular Engineering, University of Connecticut, 191 Auditorium Rd., Storrs, CT 06269, USA Center for Clean Energy Engineering, University of Connecticut, 44 Weaver Rd., Storrs, CT 06269, USA

ARTICLE INFO

Keywords: DFT Y Zeolite Adsorptive desulfurization Ion-exchanged Y GuCeY

ABSTRACT

Sulfur compounds present in petroleum fuels are a significant contributor to environmental pollution through the formation of sulfur oxides during combustion. To mitigate release of these pollutants by reducing the sulfur content of transportation fuels, adsorptive desulfurization (ADS) under ambient conditions has been studied. Sorbent materials, in particular Cu and Ce ion-exchanged Y (CuCeY), have exhibited excellent ADS performance, however, the basis for this improved adsorption has not been fully understood. For this purpose, Density Functional Theory (DFT) calculations investigated the adsorption mechanisms of thiophenic sulfur on CuCeY. Calculated adsorption enthalpies ΔH_{ads} agree with experimental results, indicating exothermic adsorption strength following the order of: Y < CeY < CuY < CuCeY. The preferential adsorption mechanism is via π -complexation between Cu and π -bonded C = C in the adsorbate. Natural Bond Orbitals (NBOs) further studied the electronic interactions during adsorption, and demonstrated synergy between Cu and Ce cations via electron sharing. Bonding and antibonding NBO pairs between Cu and adsorbed sulfur combined with significant delocalizations of the electronic structure provides further reasoning for the superior adsorption of sulfur on CuCeY.

1. Introduction

Desulfurization is an important process to produce clean fuels as we strive to minimize the harmful effects of fossil fuels. Naturally occurring sulfur compounds in crude oil introduce a variety of issues in refinery processing including corrosion and catalyst poisoning. [1] Additionally, sulfur that persists through refinery treatment to gasoline, diesel, and jet fuels contributes negatively to public health and the environment. [2] With combustion of these fuels, sulfur molecules readily form SO_x , which is a precursor for acid rain and a contributor to air pollution, causing environmental and human health problems. [3,4] In response to these concerns, the United States (US) Environmental Protection Agency (EPA) has set sulfur limits of 10 ppm in gasoline and 15 ppm in diesel fuels. [5,6] Even lower sulfur levels near zero must be accomplished for fuel cell applications, as sulfur molecules cause catalyst poisoning and deactivation, leading to decreased overall efficiency of the cell. [7].

To reduce sulfur contents to acceptable levels, adsorptive desulfurization (ADS) is a promising technology to produce zero sulfur fuels at ambient conditions. [8] This offers many benefits over other desulfurization technologies, as ADS avoids the high temperature and H₂

pressure required by hydrodesulfurization (HDS) and the long processing times of oxidative desulfurization (ODS).[9,10] ADS relies on effective materials to selectively adsorb sulfur molecules from transportation fuels including zeolites, metal oxides, metal organic frameworks (MOFs), and carbon materials.[10] One such promising material is metal exchanged Y zeolite. This is due to the Faujasite (FAU) framework of Y with its porous structure containing large 7.4 Å openings to a 11.2 Å supercage suitable for easy transport and diffusion of adsorbate molecules.[11,12] In addition, Brønsted acid sites and high surface area provide active sites for the adsorption of sulfur.[13].

Additional steps including metal ion-exchange have been used to further improve the desulfurization characteristics of Y by increasing the adsorption capacity and selectivity for sulfur in the presence of competing adsorbates. Ion-exchange with Cu and Ce has demonstrated increased adsorption of thiophenic sulfur compounds such as thiophene (TP) and benzothiophene (BT) in model gasoline and diesel fuels. [14,15] Previous studies have demonstrated that both Brønsted acid site exchanged ions and metal species within the Y supercage can effectively adsorb sulfur. [16] The inclusion of both Cu and Ce in bimetallic CuCeY has shown superior adsorption properties attributed to the placement of

^{*} Corresponding author at: 191 Auditorium Road, Unit 3222, Storrs, CT 06269-3222, USA. *E-mail address:* ioulia.valla@uconn.edu (J.A. Valla).

ions within the zeolite and synergistic effects between the two metals. [15,17–19] Our recent work using x-ray adsorption spectroscopy (XAS) has found Cu species occupying adsorption sites accessible to the supercage and Ce located in interior sites within the Y zeolite framework.[20] With this configuration, CuCeY has exhibited both the high sulfur capacity of CuY and the selectivity characteristic of CeY.[19,21] Furthermore, mesoporosity has been introduced in metal exchanged Y materials to overcome the diffusion limitations of large sulfur compounds such as dibenzothiophene (DBT) and dimethyldibenzothiophene (DMDBT).[18,22] Additionally, ADS sorbents including Y zeolite have shown reusability after regeneration with only a slight decrease in sulfur capacity.[23] In fact, over 90% of sulfur capacity was retained after thermal regeneration of CuY[24], and no significant DMDBT capacity loss was reported after two regeneration cycles of mesoporous CuCeSAY [18]. In our previous work, sulfur breakthrough curves show the increased capacity for BT and DBT of CuCeY and CuCeSAY compared to the parent Y, CeY, and CuY sorbents.[22] These findings provide the premise for the present computational study examining the adsorption mechanism on these materials.

Two primary adsorption modes have been observed for sulfur compounds on ion-exchanged Y zeolites: π -complexation and direct sulfurmetal (S-M) interaction. Either π -complexation or S-M bonding may be favored depending on the type and oxidation state of the exchanged ions.[25] Many transition metal ions including Cu⁺ cations have shown the ability to form strong π -complexes with thiophenic sulfur compounds due to available 4 s orbitals for σ -type bonding, and occupied 3d orbitals for back donation of electron density to the antibonding π -orbitals of the C = C bonds in the sulfur ring. [26–28] π -complexation has also been found between sulfur molecules and ion-exchanged rare earth metals, in addition to S-M bonding.[29-31] These mechanisms have been demonstrated through in-situ IR measurements during temperature programmed desorption of sulfur from zeolite samples.[18,22] In these studies, the thiophenic sulfur C = C peak at 1570 cm⁻¹ was shown to shift to a lower frequency due to a loss of electron density when adsorbed on Cu containing zeolites. This indicates adsorption through $\boldsymbol{\pi}$ interactions between the adsorbate C = C bond and ion-exchanged Cu. Conversely, with Ce exchanged Y samples, the C = C peak at 1450 cm⁻ was shifted to a greater frequency due to increased electron density of the thiophenic conjugated ring. This, in addition to peaks due to stretching of sp3 C-H bonds, provides evidence for S-M interactions in Ce zeolites. The combination of both adsorption modes has been suggested as a reason behind the high adsorption capacity and selectivity of CuCeY.[19] Desorption of sulfur from CuCeY occurred at higher temperature than from CuY and CeY, indicating a stronger affinity for sulfur in the bimetallic system. [22].

Previous work has investigated the kinetics and thermodynamics of sulfur adsorption of metal exchanged Y zeolites. Jiang et al. used batch experimental data to study the kinetics and thermodynamics of DBT adsorption on NaY. [32] They calculated adsorption enthalpy (ΔH_{ads}) of -30.3 kJ mol $^{-1}$ and found that the process can be described by either the Langmuir or pseudo-second-order model. The adsorption capacity was found to increase while the Langmuir constant decreased at higher temperature. For the pseudo-second-order model both capacity and the kinetic parameter increased with increasing temperature. In addition, they reported competitive adsorption of naphthalene over DBT due to electronic and steric effects. Similar studies were done by Song et al. for BT adsorption on CuCeY.[33] They found that BT adsorption on CuCeY follows either the Langmuir adsorption model or the pseudo-first order model, with the maximum adsorption capacity increasing with greater initial BT concentrations at higher temperatures. With the Langmuir model, the equilibrium isotherm showed that maximum capacity increased and the Langmuir constant decreased at higher temperature. For the pseudo-first-order adsorption model both capacity and the kinetic constant increased with temperature. The maximum BT removal of 99.2 % was found at 50 °C with equilibrium achieved relatively quickly at 100 min. In addition, they reported ΔH_{ads} of -26.221 kJ mol⁻¹,

indicating an exothermic process. To further examine the thermodynamics of sulfur adsorption on metal-exchanged Y, we used density functional theory (DFT) calculations to obtain ΔH_{ads} values for a number of sulfur compounds on various Y zeolite models.

Other studies have successfully used DFT to investigate adsorption on model zeolites. In particular, Gao et al. examined the adsorption of TP, BT, and DBT on NaY and several rare earth Y materials including LaY, CeY, PrY, and NdY using a 12 T (Si/Al) Y zeolite model. [30] They found that thiophenic compounds adsorbed on rare earth Y exhibit a lying configuration and interact via π -electrons of the thiophene ring and metal ion. This is in contrast to the stand-up configuration observed for BT adsorbed on NaY, suggesting differences in the adsorption mechanism. For the rare earth ion-exchanged Y, analysis of the Mulliken charges indicated that adsorption energy is dependent on the charge transfer between the sulfur molecule and the exchanged ion, with the main interaction occurring through π -electrons. Hessou et al. conducted similar research using a periodic 144 atom Y zeolite model for DFT calculations.[34] They studied adsorption of TP and benzene on the Lewis acid sites of Y as well as various ion-exchanged metal cations. For their ion-exchanged Y models, Cu(I)Y exhibited the greatest affinity for thiophene with interaction between Cu and the aromatic ring. Other similar studies have used DFT to investigate adsorption of TP and DBT on silica gel[35] and H₂S on ZnY, NiY, and GaY[36].

Our previous work has shown that differences in the locations of exchanged ions between mono- and bi-metallic systems may contribute to the varying sulfur adsorption performance. [15,20] However, it is our hypothesis that electronic interactions between Cu and Ce ions also contribute to improved binding of thiophenic sulfur, which contributes to greater desulfurization. The present work uses DFT calculations to investigate the thermodynamics of sulfur adsorption on several Y zeolite models, as well as to examine the adsorption mechanisms favored by different ion exchanged metals. In addition, natural bond orbital (NBO) calculations shed light on the electronic structure of exchanged metal cations in Y and the electronic interactions with sulfur molecules.

2. Methods

DFT simulations were done using Gaussian 16 software on the UCONN high performance computing (HPC) facilities. [37] The Y zeolite model was constructed from a two-layer ONIOM framework including a high-level quantum mechanics (QM) layer and a lower-level molecular mechanics (MM) layer. Areas of specific interest including adsorbate molecules, exchanged metal ions, and the nearby zeolite framework were treated at the QM level, while more distant atoms used the MM level to decrease computation time. The QM level includes a total of 64 out of the 172 T atoms used in the zeolite model, with the remaining 108 T in the MM layer. Similar ONIOM model setups have been used previously for theoretical study of the Cu sites in Y.[38,39] The zeolite model of CuCeY is shown in Fig. 1, and the models of the other zeolites HY, NaY, CuY, and CeY can be found in Figure S1. Components illustrated as ball-and-stick type atoms were treated at the QM level, while wireframe components used the MM level. The QM layer used the B3LYP functional[40,41] and the 6-31G(d,p) basis set,[42-46] while the MM layer used the Universal Force Field (UFF) for calculation.[47] In order to account for the many valence electrons of Ce, all Ce atoms were treated with the Stuttgart RSC 1997 effective core potential rather than the 6-31G(d,p) basis set.[48,49] Calculations of various adsorbate molecules as shown in Fig. 2 were done at the QM level with the same B3LYP 6-31G(d,p) method. These adsorbates were then placed within the supercage of the Y zeolite models and geometric optimization found the most favorable adsorption geometries. After optimization ΔH_{ads} values were obtained using the expression in Equation (1).

$$\Delta H_{ads} = H_{adsorbate+zeolite} - H_{zeolite} - H_{adsorbate} \tag{1}$$

Zeolite models were constructed using an original FAU framework

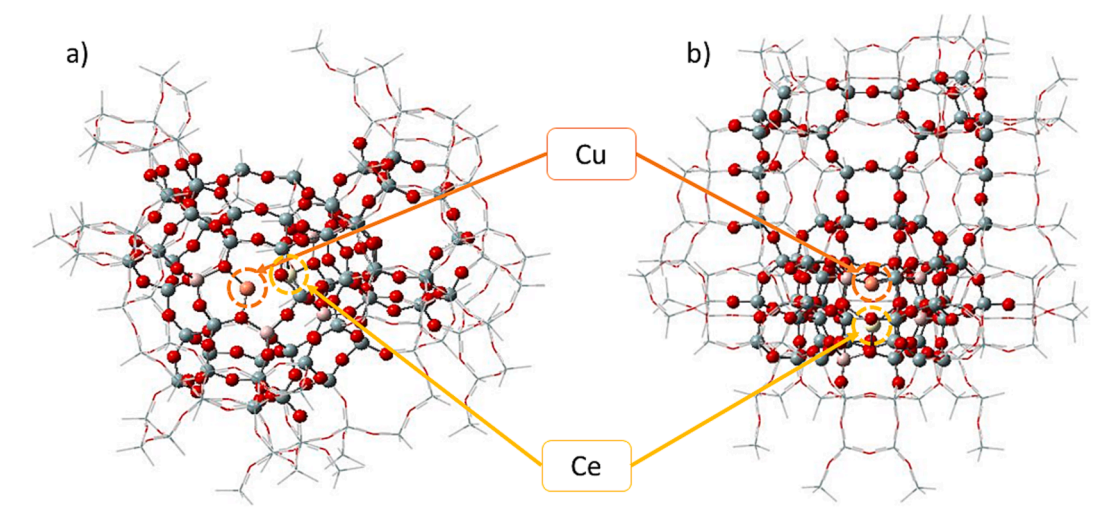


Fig. 1. DFT model of CuCeY top view (a) and side view (b) with Cu in site IÍ and Ce in site Í. The Cu atom is shown in orange and the Ce in yellow. The zeolite framework is made up of O in red, Si in grey, and Al in pink, the H atoms used to cap the exposed ends are shown as part of the wireframe. (For interpretation of the references to colour in this figure legend, the reader is referred to the web version of this article.)

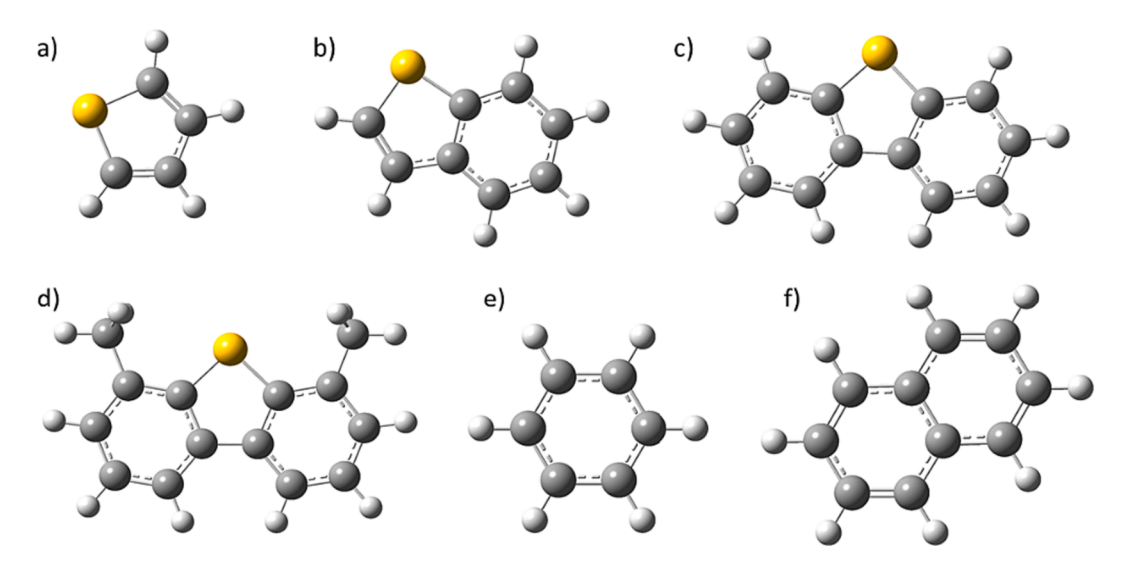


Fig. 2. Adsorbate molecules including TP (a), BT (b), DBT (c), 4,6-DMDBT (d), benzene (e), and naphthalene (f). Sulfur atoms are shown in yellow, carbon in grey, and hydrogen in white. (For interpretation of the references to colour in this figure legend, the reader is referred to the web version of this article.)

consisting of only Si and O atoms. The unit cell model was slightly reduced by removing sections furthest from the areas of interest to lower the required computation time, obtaining the 172 T subsection used as our computational model. The terminal ends of the framework were capped with H atoms to ensure charge neutrality of the system. To this starting framework, Al atoms were added in exchanged for Si as necessary to obtain the desired oxidation states of exchanged metal ions. Framework Al exists in a + 3 oxidation state in zeolites and as such each atom induces a negative charge that will be balanced by a positive charge on an exchanged metal cation.[50] Therefore, the number of Al atoms added is equivalent to the total of the desired oxidation states of all exchanged metal cations with one Al added for Cu⁺ and 3 Al for Ce³⁺. Al locations were chosen in the QM layer nearby to the cation sites with care to obey Löwenstein's rule avoiding Al-O-Al centers. [51] While the resulting Si/Al ratio of this computational model differs from physical Y samples, previous computational studies have found that the electronic properties of ion-exchanged metals in Y are not particularly sensitive to the Al distribution.[52] Spin multiplicity of each zeolite model was determined based on the oxidation state of the exchanged cations as no unpaired electrons are expected from framework atoms. The HY, NaY,

and CuY models were assigned a singlet spin state as H^+ , Na^+ , and Cu^+ contain only paired electrons. Conversely CeY and CuCeY require a doublet spin state due to the unpaired valence electron of Ce^{3+} .

After building the models of ion-exchanged Y zeolites HY, NaY, CuY, CeY and CuCeY, the geometries were optimized to find the most stable configuration of the exchanged metals within the frameworks. Initial placement of metal cations has been discussed previously and was based on findings from previous studies. [20] For all of the zeolite models, geometric optimization did not disturb the location of the cation sites due to the relative stability within the six-member rings. Following optimization of the models, frequency calculations were used to determine thermodynamic properties including the enthalpies provided in Table S6, and NBO calculations examined the electronic structure of each zeolite. The same calculations were done for the adsorbate molecules shown in Fig. 2 including thiophenic S compounds and aromatics found in gasoline, diesel, and jet fuels.

3. Results

3.1. Electronic structure of Ion-Exchanged zeolites

Prior to examining the adsorption mechanisms on metal ionexchanged Y zeolites, the electronic structures of the vacant Y models, in particular the exchanged cations, were studied. The DFT calculated Natural Population Analysis (NPA) gives significant information about the charge and electron distribution of the theoretical models. The natural electron configuration as shown in Table 1 gives the valence electrons of Cu and Ce in monometallic and bimetallic Y. The electron valence is a useful tool to predict the potential bonding mechanisms with sulfur compounds. Cu ions in CuY and CuCeY should have occupied 3d orbitals and available 4 s orbitals to allow for π -complexation adsorption given the Cu⁺ valence of [Ar]3d¹⁰. As shown in Table 1, the computed Cu electronic configuration in CuY is [Ar]3d $^{9.68}$ 4 s $^{0.31}$ and similarly in CuCeY it is [Ar]3d^{9.57}4 s^{0.31}. In both models Cu has a calculated natural charge close to + 1, at + 0.95 in CuY and + 1.07 in CuCeY. This electron configuration allows for both π -complexation and direct S-M σ type bonding interactions between the Cu and adsorbed

For Ce, the computed natural charges in CeY and CuCeY are both around 2 e, at 2.06 e in CeY and slightly reduced to 1.92 e in CuCeY. In CeY, the Ce ion has an electron configuration [Xe]4 ${
m f}^{1.18}5{
m d}^{0.47}5{
m f}^{0.17}$ with miniscule occupation of 7 s and 6d orbitals. This occupancy of d and f orbitals might be attributed to the overlap of the large d and f orbitals with the framework electronic structure. A similar effect is seen with Ce CuCeY, with the computed electron structure of [Xe] $4f^{1.20}5d^{0.45}5f^{0.16}6d^{0.15}$. Here there is also slight occupancy of 0.15 e⁻ in the 6d orbital resulting in a lower computed natural charge of 1.92 e. In this case, interactions between Cu and Ce may account for the even greater electron density near Ce and suggests some synergy between the two exchanged cations. The same was found for a model of CuCeY with 5 framework Al as described in Table S1. Sharing of electron density between the Y framework and Ce is evident for the second order perturbation stabilizations given in Table S2 with significant stabilizations from oxygen lone pair (LP) or bonding (BD) O-Si and O-Al donors to the unoccupied valence (LV) orbitals of Ce. In addition to stabilizing the overall structure of CeY and CuCeY, these perturbations of the Lewis structure contribute to additional electron density near the Ce cation, influencing the natural charge. Overall, the lack of fully occupied valence s, p and d orbitals on the Ce cations may suggest an adsorption mechanism other than direct S-M interaction or π -complexation on Ce. While 4f orbitals have generally been considered inactive in chemical bonding, in lanthanide elements 4f orbitals have been found to hybridize with other s, p and d orbitals, potentially contributing to bonding with adsorbed sulfur compounds.[53,54].

In addition to NPA analysis of the model zeolites, the synergy between Cu and Ce in CuCeY was further examined through calculations of the NBOs between the two metals. As shown in Table 2, there are computed NBOs including BD and antibonding (BD*) orbitals between Cu and Ce. The BD NBO is primarily (93.4%) due to contributions from Cu orbitals with only slight contribution (6.6%) from Ce. Hybridization of the Cu contribution shows 94.1% from 3d orbitals compared to 5.6%

 $\begin{tabular}{ll} \textbf{Table 1} \\ \textbf{Natural electron structure of ion-exchanged metals Cu and Ce in Y zeolite models.} \\ \end{tabular}$

	Atom	Natural Charge, e	Natural Electron Configuration (Occupancy)
CuY	Cu	0.95	[core]4s(0.31)3d(9.68)4p(0.04)
CeY	Ce	2.06	[core]6s(0.00)4f(1.18)5d(0.47)7s(0.07)5f (0.17)6d(0.05)
CuCeY	Cu	1.07	[core]4s(0.31)3d(9.57)4p(0.04)
CuCeY	Ce	1.92	[core]6s(0.07)4f(1.20)5d(0.45)6p(0.03)5f (0.16)6d(0.15)

for the 4 s orbital. This indicates the NBO is composed of donation of electron density from Cu 3d orbitals to Ce. From the Ce hybridization, this shared electron density is split among several different orbitals, with the majority on 4f and 5d. This apparent synergy between Cu and Ce in CuCeY has been previously suggested as one of the reasons for its increased ADS capacity.[19] The synergy is further highlighted by the second order perturbation theory stabilizations between Cu and Ce given in Table S3. Electron delocalization from lone pairs of Cu to unoccupied orbitals of Ce are evident and improve the stability of the overall system.

Fig. 3 shows two NBOs between Cu and Ce in the CuCeY zeolite model corresponding to the BD and BD* NBOs described in Table 2.A large portion of the 172 T framework has been removed for easier visibility of the active site. The electron density of the BD NBO is widely distributed around Cu and its six-member ring with only slight distribution centered on Ce. Conversely, the BD* NBO electron density is centered on the Ce cation, with some electron density centered on Cu.

3.2. Adsorption

Following computational study of the vacant ion-exchanged zeolite models, adsorption calculations were done to determine the interactions between the zeolites and adsorbate molecules. Sulfur molecules including TP, BT, DBT and DMDBT were placed in various configurations within the supercage of the ion-exchanged Y zeolite models and the geometries were optimized to find stable adsorption modes. After optimization of the adsorption geometries, frequency calculations were used to determine thermodynamic properties of the sulfur-zeolite adsorption complex.

As mentioned previously, several different adsorption mechanisms have been reported for sulfur on metal ion-exchanged Y including direct S-M bonding and π -complexation on ion-exchanged Cu $^+$. By altering the initial positioning of sulfur compounds in the supercage, models of these adsorption mechanisms on the Cu containing zeolites, CuY and CuCeY, have been generated as shown in Fig. 4. BT was chosen as a representative sulfur compound to examine the different adsorption mechanisms for thiophenic sulfur. The η^2 coordination with two C atoms of the sulfur molecule can be clearly seen, suggesting π -complexation, as well as the interaction between S and Cu suggesting the S-M mechanism.

Comparison between the ΔH_{ads} values for BT on CuY and CuCeY with S-M bonding and π -complexation can determine the more favorable mechanism for ADS on Cu⁺ based sorbents. Table 3 shows the increase in magnitude of ΔH_{ads} with π -complexation compared to S-M interaction. Adsorption on CuY is improved from ΔH_{ads} of -98 kJ/mol with S-M bonding to -147 kJ/mol with π -complexation. Likewise, ΔH_{ads} is improved from -177 kJ/mol with S-M interaction to -234 kJ/mol in a π -complexation configuration on CuCeY. These represent significant increases in the adsorption strength of sulfur compounds with the more favorable π -complex. As the computed ΔH_{ads} values with the S-M mechanism are still significantly exothermic, there is potential for adsorption via both mechanisms in a physical system.

Attempts to optimize CeY with S molecules in the supercage show an absence of stable adsorption geometries in both the S-M and π configurations found for Cu containing zeolites. While S-M σ bonding has been reported on Ce(IV)Y, adsorption on reduced Ce sites appears to follow a different mechanism. [55] For CeY, stable adsorption of thiophenic sulfur was found with cyclic structures centered over the Ce cation with the adsorbate lying flat, parallel to the Ce six-member ring site. This mechanism was found with both η^5 coordination between Ce and the thiophene ring, and η^6 coordination with a benzene ring as shown for BT in Fig. 5.

In addition to investigating the adsorption mechanism of BT on CuY, CeY and CuCeY, other sulfur compounds TP, DBT and DMDBT have also been considered. Fig. 6 shows the most stable adsorption geometries of the four sulfur compounds on CuCeY. All show similar η^2 coordination between the Cu $^+$ ion and two $\pi\text{-bonded}$ C atoms of the sulfur molecule,

Table 2Bonding NBOs between Cu and Ce ions in CuCeY.

NBO	α Occupancy	β Оссирансу	Contribution	Polarization Coefficient, c_A	Hybridization
BD Cu-Ce	0.99	0	Cu 93.4%	0.97	4 s(5.6%) 3d(94.1%)
			Ce 6.6%	0.26	6 s(13.4%) 6p(9.8%) 5d(36.9%) 4f(39.9%)
BD* Cu-Ce	0.02	0	Cu 6.6%	0.26	4 s(5.6%) 3d(94.1%)
			Ce 93.4%	-0.97	6 s(13.4%) 6p(9.8%) 5d(36.9%) 4f(39.9%)

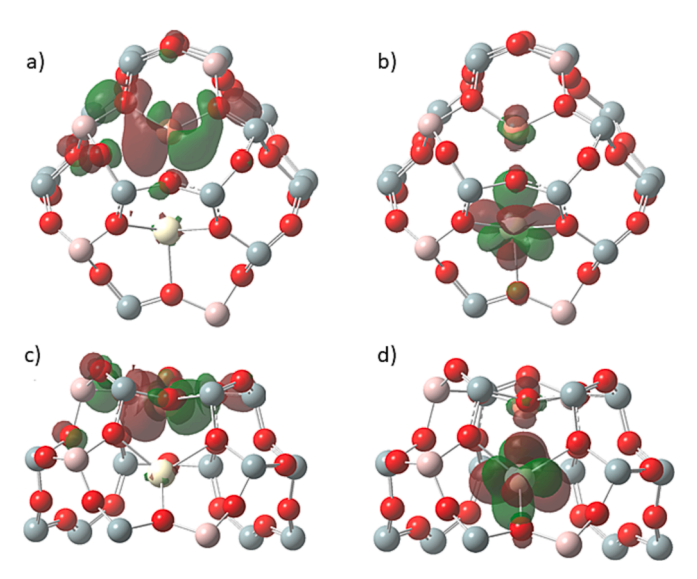


Fig. 3. Selected NBOs involving Cu and Ce of CuCeY including BD Cu-Ce NBO top view (a) and side view (c), and BD* Cu-Ce NBO top view (b) and side view (d).

as expected with π -complexation. The same is true for non-sulfur aromatics benzene and naphthalene as shown in Figure S2. The adsorption geometries of the sulfur molecules and aromatics on the other zeolite models are given in the Figures S3-S6.

For each zeolite model and adsorbate, the most favorable adsorption mode has been used with Equation (1) to calculate adsorption enthalpies as given in Table 4 and shown in Fig. 7. The results largely agree with previously reported findings showing theoretical adsorption strength following the same trend as experimental capacity of CuCeY > CuY > CeY > parent Y.[8,14,22] For HY and NaY the adsorption enthalpy depends largely on the size of the sulfur compound with adsorption strength following DMDBT > DBT > BT > TP on HY and DBT > DMDBT > BT > TP for NaY. The adsorption enthalpies are comparable between NaY and HY, with the exception of DMDBT which shows a 20 kJ/mol stronger interaction on HY. Aromatics benzene and naphthalene have also been considered to examine the selectivity of the zeolites for sulfur. On HY, adsorption enthalpies of -56 and -61 kJ/mol were calculated for benzene and naphthalene, respectively. With NaY, ΔH_{ads} is -60 kJ/mol for benzene and -73 kJ/mol for naphthalene. Results for both zeolites indicate slight selectivity towards sulfur containing molecules over aromatics. Comparing monocyclic adsorbates, adsorption strength is stronger for benzene than thiophene on both HY and NaY by about 5 kJ/mol. However, BT and larger sulfur compounds indicate selective adsorption over benzene due to greater magnitude of adsorption enthalpy. The same is seen for the larger diesel range sulfur molecules DBT and DMDBT that show increased adsorption strength compared to naphthalene.

For CuY and CeY, the adsorption enthalpies are relatively consistent regardless of sulfur compound, with variation of only about 10 kJ/mol. The ΔH_{ads} values range from -140 to -150 kJ/mol on CuY and between -125 to -135 kJ/mol on CeY. This shows that the adsorption is dominated by the interaction between the exchanged metal cation and sulfur

molecule, while effects from the adsorbate size are insignificant. In fact, there is no apparent trend based on adsorbate size observed on CuY and CeY with a difference in ΔH_{ads} of less than 3 kJ/mol between the smallest compound, TP, and the largest, DMDBT. Both CuY and CeY indicate some selectivity for sulfur compounds over benzene, with ΔH_{ads} of -125 kJ/mol on CuY and -118 kJ/mol on CeY. The decreased magnitude of these ΔH_{ads} values compared to the sulfur containing molecules suggests selectivity for sulfur adsorption over competing aromatics in gasoline fuels. Conversely, little difference is found between the adsorption enthalpies of naphthalene and the larger sulfur compounds on CuY and CeY. ΔH_{ads} of naphthalene on CuY is calculated at -143 kJ/mol, comparable to the values of -143 and -142 kJ/mol for DBT and DMDBT, respectively. The same is true for CeY where the ΔH_{ads} for naphthalene of -130 kJ/mol is comparable to the values of -125 and -133 kJ/mol for DBT and DMDBT.

Adsorption on CuCeY follows a similar pattern to CuY and CeY with ΔH_{ads} values independent of adsorbate size, and adsorption strength instead following DMDBT > BT > DBT > TP. However, there is some variation in the calculated values from TP at -201~kJ/mol to DMDBT at -249~kJ/mol. Adsorption strengths for BT and DBT are within that range at -234~and~217~kJ/mol, respectively. As with CuY and CeY, the presence of an S atom in the adsorbate molecule does not lead to preferential adsorption when compared to aromatics benzene and naphthalene. The calculated ΔH_{ads} of -228~kJ/mol for benzene and -233~kJ/mol for naphthalene are comparable to the sulfur containing molecules. These values suggest that the improved ADS performance with the addition of Cu and Ce into Y should be attributed to stronger chemisorption and a greater number of available adsorption sites leading to higher capacity, rather than increased selectivity for sulfur over aromatics.

In addition to the thermodynamic properties of ADS on Cu and Ce exchanged Y, the physical morphology of the active sites can give insight into the adsorption performance. Fig. 8 shows the active site of CuCeY with the surrounding framework removed both as a vacant site and with adsorbed BT. When the site is vacant, the Cu cation can be observed centrally located within the six-member ring and slightly below the plane of the ring towards the sodalite cage. However, this position becomes significantly distorted with BT adsorption. When interacting with π -bonded carbons of BT, the Cu cation has migrated laterally and up into the supercage above the six-member ring site. This movement is clearly evident from the Cu-O bond distances given in Table 5. Distinction has been made between distances from Cu to the nonequivalent O2 and O3 sites in the six member ring of the FAU structure. With adsorption of CuCeY, there is a significant increase of 1.53 and 1.85 Å in two of the Cu-O2 bond distances, and a slighter increase of 0.24 Å for the third O2 atom. While the overall greater bond distances are due to movement of Cu above the plane of the ring structure, the disparity in the changes is due to the Cu cation shifting out of the center of the ring and closer to one side. Hence the Cu-O2 distance of 2.16 Å for the closest O2 atom compared to 3.52 and 3.90 Å to the other two. Additionally, two of the Cu-O3 distances are decreased by 1.02 and 0.38 Å, while the other is slightly greater than prior to adsorption, further illustrating the lateral movement of the Cu cation.

This effect is also seen in CuY, with a maximum shift in Cu-O2 distance of 0.40 Å, and the greatest change in Cu-O3 distance of 0.21 Å. In CeY only miniscule changes in Ce-O2 and Ce-O3 distances are observed, with the exception of one Cu-O3 length increased by 0.52 Å. The

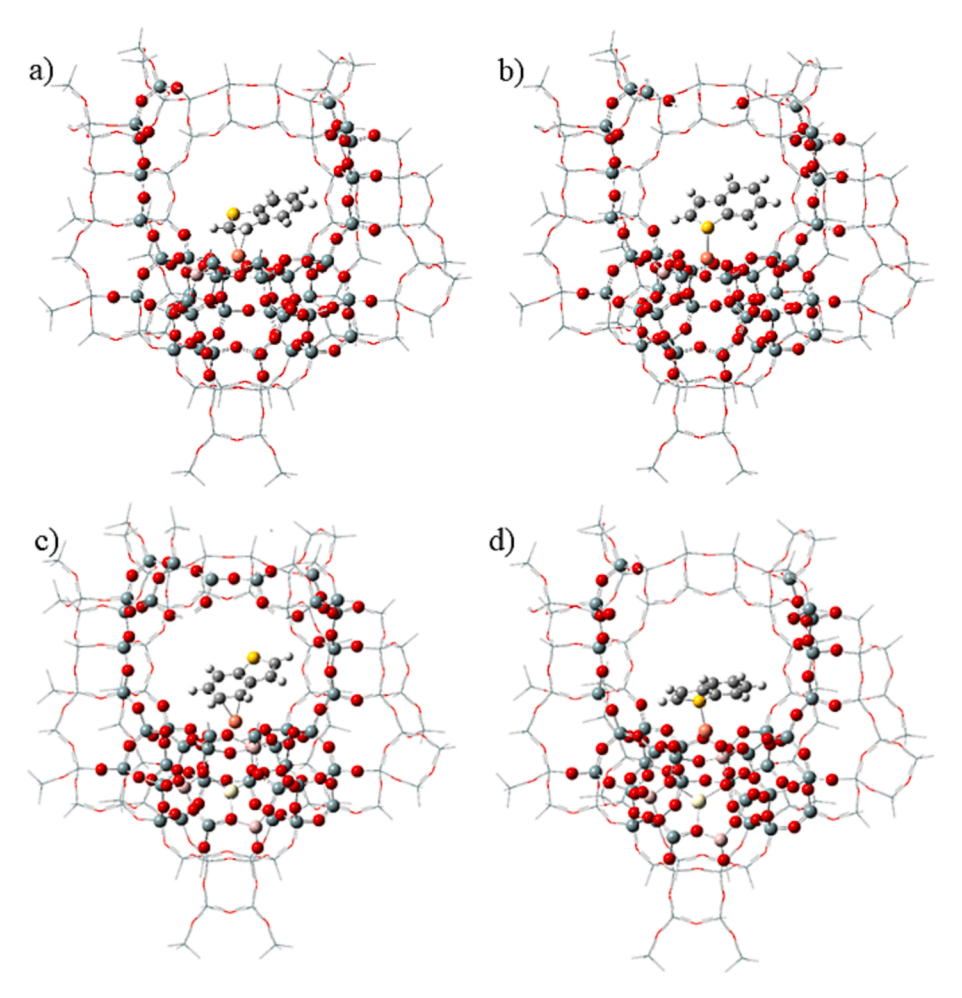


Fig. 4. Adsorption mechanisms of BT on Cu in CuY and CuCeY. BT can be adsorbed on CuY via π -complexation (a) and direct S-M interaction (b), and on CuCeY via π -complexation (c) and direct S-M interaction (d).

Table 3 Adsorption enthalpies of BT on CuY and CuCeY with different mechanisms.

Zeolite	CuY		CuCeY		
Mechanism	S-M	π	S-M	π	
ΔH _{ads} (kJ/mol)	-98	-149	-177	-234	

movement of the Cu cation into the supercage to occupy a more favorable position for adsorption has also been shown experimentally using XAS and Rietveld Refinement which indicated that Cu was mostly located in the supercage site II while Ce occupied mostly the interior framework locations.[15,20].

3.3. Electronic changes with adsorption

The ADS process on ion-exchanged Y can be further studied by considering the electronic interactions between zeolite and adsorbate, with BT used as the model sulfur compound. Table 6 shows the changes in natural atomic charge of selected atoms involved in the adsorption process on the metal ion-exchanged zeolites CuY, CeY, and CuCeY. With the π -complexation adsorption mechanism on Cu, the net change in charge on each atom is minimal due to balancing σ -donation of electron density from the C = C of BT to the Cu 4 s orbital and back donation from the 3d orbitals of Cu to the C = C π^* orbital. With BT adsorption on CuY this results in a net change in atomic charge of 0.21 e on Cu and around -0.2 e on the two C atoms involved in the π -complex and is accompanied by lengthening of the 1.36 Å C = C bond to 1.41 Å C–C. There is

insignificant change in the charge on the sulfur atom of BT as it is not directly involved in the interaction with Cu. In the case of CeY there is a decrease in the natural atomic charge on Ce from 2.06 e to 1.83 e with adsorption. This suggests further delocalization of electron density towards Ce when interacting with BT. For BT, the change in the average natural charge of the six-member ring carbons in BT is near zero, however the charge on sulfur is slightly increased from 0.41 to 0.55 e, due to further sharing of the S electrons with adsorption of BT on CeY.

The changes in natural atomic charge with adsorption of BT on CuCeY follow a similar pattern to the adsorption on CuY. As with CuY, there is a slight increase in the natural charge of Cu from 1.06 to 1.14 e, and conversely the charges on the two C atoms involved in the $\pi\text{-complexation}$ are slightly decreased by -0.21 e. The bond distance between the two carbons closely interacting with Cu increases from 1.39 to 1.43 Å with the change from sp^3 to sp^2 hybridization due to the $\pi\text{-complex}$ formation. In addition, while the adsorption of BT occurs on the Cu atom, Ce in CuCeY also shows a change in calculated natural charge from 1.92 to 2.07 e.

In addition to natural atomic charge, NBOs can be used to examine interactions between atoms in the zeolite adsorption model. Table 7 shows the primary NBOs between the Cu atom of CuY and adsorbed BT. Both BD and corresponding BD* orbitals have been found between ion-exchanged Cu and C of BT. The BD orbital is fully occupied with two electrons, with primary contribution around 74% from Cu 3d orbitals, and the remaining contribution mostly from C 2p. The BD* orbital is only partially occupied at 0.93, about one e⁻. Contributions to the BD* orbital are opposite to that of the BD orbital, with C 2p providing about 74% of the contribution. This interaction between occupied 3d orbitals

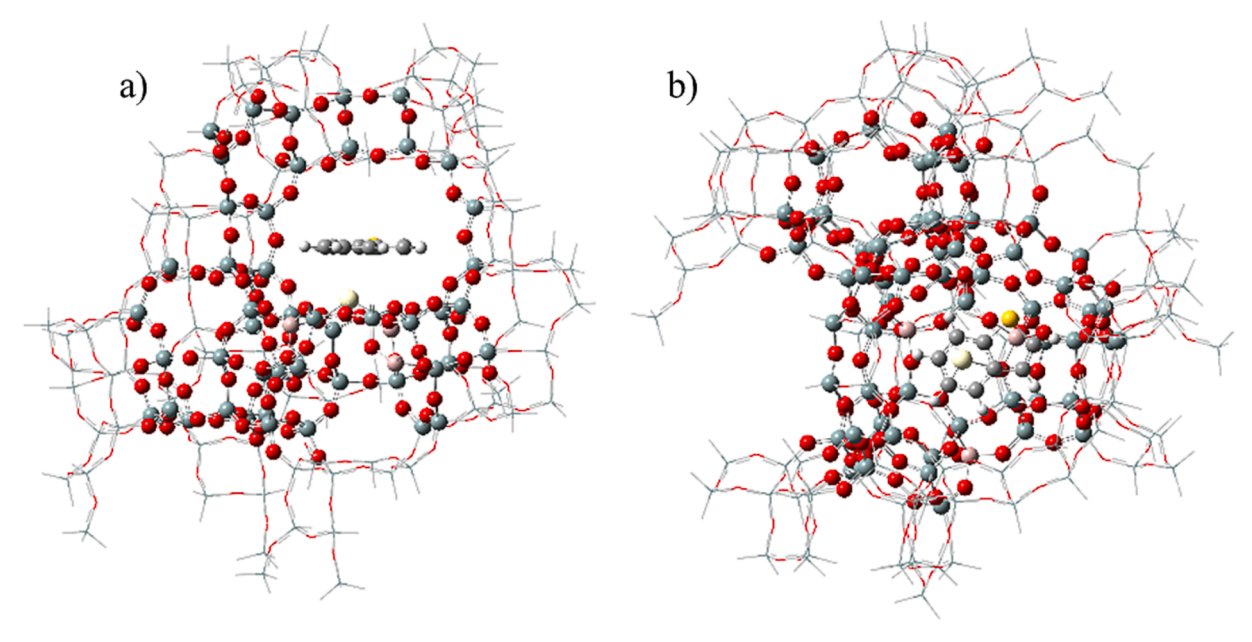


Fig. 5. Adsorption of BT on CeY showing side view (a) and top view (b). The preferred adsorption mechanism on CeY follows η^6 coordination with the benzene ring of BT centered over Ce³⁺.

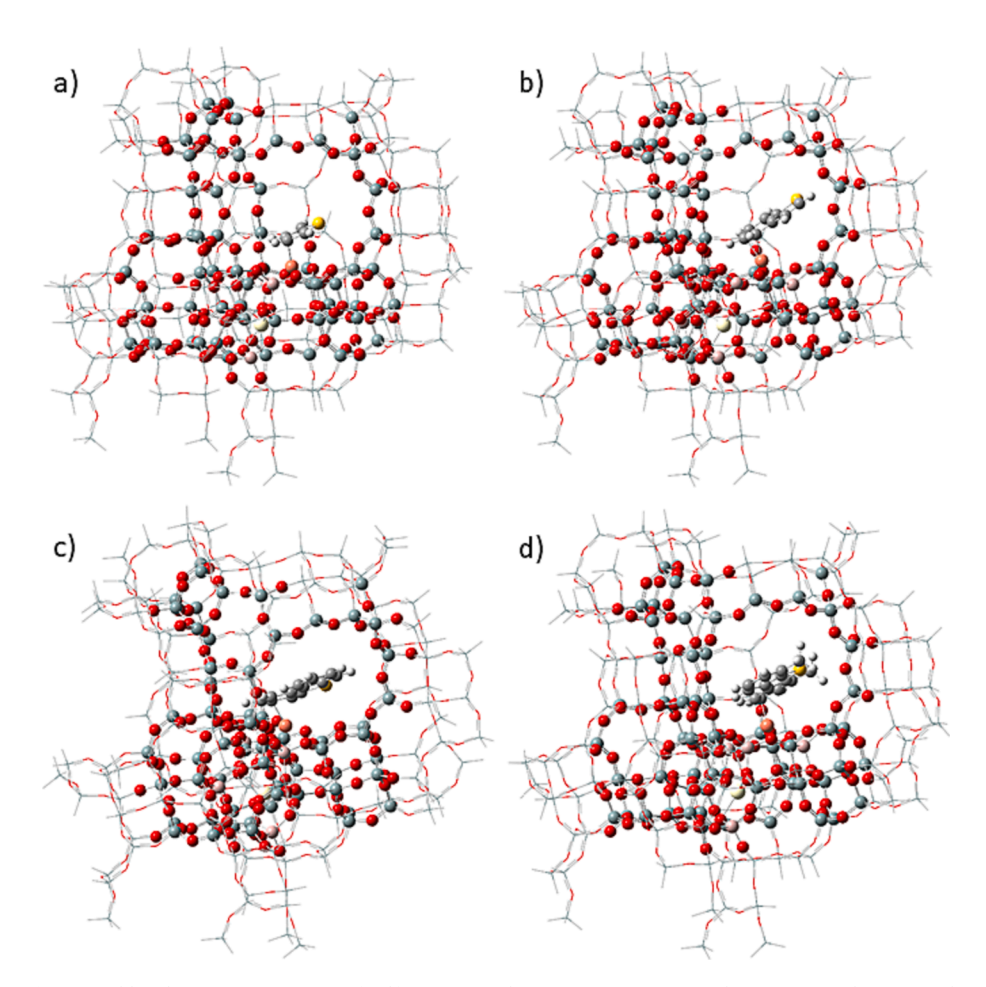


Fig. 6. Stable adsorption geometries of sulfur compounds on CuCeY: TP (a), BT (b), DBT (c) and DMDBT (d).

of Cu and the 2p orbitals of C is consistent with the expected $\pi\text{-complexation}$ adsorption mechanism. On the other hand, with BT adsorption on CeY in a η^6 coordinated interaction, no NBOs between the cation and adsorbate were found.

As has been given for CuY, Table 8 shows the NBOs between Cu and BT for adsorption on CuCeY. Once again there are singular BD and BD* orbitals between the Cu cation and C of BT. Due to the presence of Ce, the doublet spin state was used in calculation so both α and β

Table 4Adsorption enthalpies of the strongest adsorption geometry of several adsorbate molecules on parent and ion-exchanged Y models.

	Adsorption Enthalpy, ΔH_{ads} (kJ/mol)								
Zeolite	TP	BT	DBT	DMDBT	Benzene	Naphthalene			
HY	-50	-76	-96	-103	-56	-61			
NaY	-55	-72	-92	-81	-60	-73			
CuY	-141	-149	-143	-142	-125	-143			
CeY	-136	-126	-125	-133	-118	-130			
CuCeY	-201	-234	-217	-249	-228	-233			

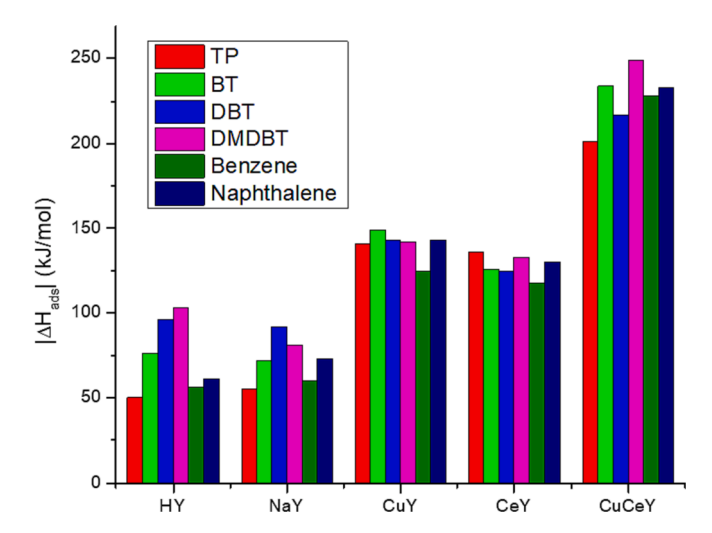


Fig. 7. Magnitude of computed adsorption enthalpies from several adsorbate molecules on Y zeolite models.

occupancies are given. The overall occupancy of the NBOs is comparable to CuY-BT with about two e^- in the bonding NBO and one in the antibonding, when considering both α and β occupancies. Primary contributions to the NBOs include Cu 3d and C 2p orbitals as expected with $\pi\text{-complexation}.$ The relative contributions of about 79% Cu 3d and 21% C 2p to the BD NBO are similar to those observed with adsorption of BT on CuY.

BD NBOs between Cu and adsorbed BT on both CuY and CuCeY are shown in Fig. 9, with most of the 172 T zeolite framework removed for easier visibility. Each corresponds to the Cu-C BD NBO described in Table 8. The electron density is well dispersed over the near entirety of the adsorbate molecule as well as around the Cu cation. The slight differences between the shape of the CuY-BT and CuCeY-BT NBOs can be attributed to the orientation of the sulfur atom of BT in regards to the Cu cation.

The electronic structure of the zeolite-adsorbate complex can be further examined through the primary delocalization of NBOs by 2nd order perturbation theory. Table 9 lists the primary stabilizing delocalizations of NBOs with the adsorption of BT on CuY and CuCeY. The stabilization energies, $\Delta E_{ij}^{(2)}$, indicate the intensity of the interaction between the donor and acceptor NBOs and point to a generally greater extent of conjugation in the system. Also reported are the energy gap between contributing NBOs, $\varepsilon_j^{(NL)} - \varepsilon_i^{(L)}$, and an interaction parameter corresponding to the overlap between the two NBOs, F_{ij} . These terms, along with the occupancy of the donor Lewis NBO, q_i , contribute to $\Delta E_{ij}^{(2)}$ as shown in Equation (2). The occupancy term, q_i , is either 1 for openshell or 2 for closed-shell systems so it is important to note the

Table 5Distortion of cation-oxygen distances in the six-member ring with adsorption of BT.

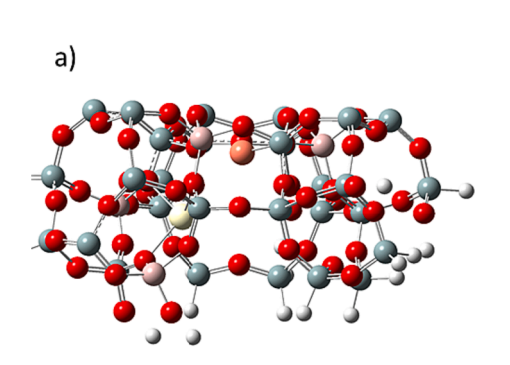
Cation			O2 dis	stance, Å		O3 dista	ınces, Å	
CuY	Cu ⁺	vacant	1.91	1.98	2.14	2.79	3.01	3.09
		w/BT	2.01	2.38	2.54	2.73	3.13	3.30
		Δ	0.10	0.40	0.40	-0.06	0.12	0.21
CeY	Ce^{3+}	vacant	2.31	2.31	2.37	2.59	2.63	2.75
		w/BT	2.36	2.37	2.43	2.54	2.58	3.27
		Δ	0.05	0.06	0.06	-0.05	-0.05	0.52
CuCeY	Cu^+	vacant	1.92	1.99	2.05	3.03	3.13	3.27
		w/BT	2.16	3.52	3.90	2.01	2.75	3.46
		Δ	0.24	1.53	1.85	-1.02	-0.38	0.19

Table 6Natural atomic charge of atoms involved in BT adsorption of CuY, CeY and CuCeY before adsorption, after adsorption and net change.

		Natural Atomic Charge, e				
	atom	Before Adsorption	BT Adsorbed	Δ		
CuY-BT	Cu	0.95	1.16	0.21		
	S	0.41	0.46	0.04		
	C1	-0.41	-0.60	-0.19		
	C2	-0.27	-0.50	-0.23		
	Cave*	-0.21	-0.20	0.00		
CeY-BT	Ce	2.06	1.83	-0.23		
	S	0.41	0.55	0.14		
	Cave**	-0.21	-0.24	-0.04		
CuCeY-BT	Cu	1.06	1.14	0.07		
	Ce	1.92	2.07	0.14		
	S	0.41	0.44	0.03		
	C1	-0.22	-0.43	-0.21		
	C2	-0.25	-0.46	-0.21		
	Cave*	-0.24	-0.23	0.01		

 $[\]ensuremath{^*}\text{average}$ of C atoms not directly interacting with Cu.

^{**}average of the 6C atoms comprising the benzene ring of BT.



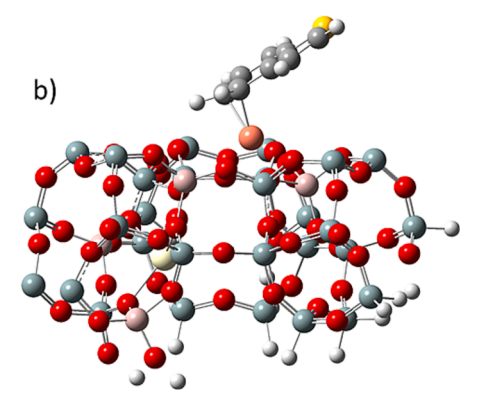


Fig. 8. Distortion of Cu cation active site in CuCeY with adsorption of BT. Vacant site (a) Cu is located centrally and slightly below the plane of the six-member ring and shifts above the place and to the side of the ring upon adsorption of BT (b).

Table 7NBO interactions between Cu and BT during adsorption on CuY.

NBO	Occupancy	Primary Hybrid	Contribution	Polarization Coefficient, c_A	Hybridization
BD Cu-C	1.96	Cu 3d	74.2%	0.86	s(0.1%) p(0.2%) d(99.7%)
		C 2p	25.8%	0.51	s(6.2%) p(93.7%) d(0.1%)
BD* Cu-C	0.93	Cu 3d	25.8%	0.51	s(0.1%) p(0.2%) d(99.7%)
		C 2p	74.2%	-0.86	s(6.2%) p(93.7%) d(0.1%)

Table 8
NBO interactions between Cu and BT during adsorption on CuCeY.

NBO	Occupancy		Primary Hybrid	Contribution	Polarization Coefficient, c_{A}	Hybridization
	α	β				
BD Cu-C	0.98073	0.98074	Cu 3d	78.80%	0.8877	s(1.34%)p(0.08%)d(98.58%)
			C 2p	21.20%	0.4605	s(4.25%)p(95.64%)d(0.11%)
BD*Cu-C	0.45664	0.45664	Cu 3d	21.20%	0.4605	s(1.34%)p(0.08%)d(98.58%)
			C 2p	78.80%	-0.8877	s(4.25%)p(95.64%)d(0.11%)

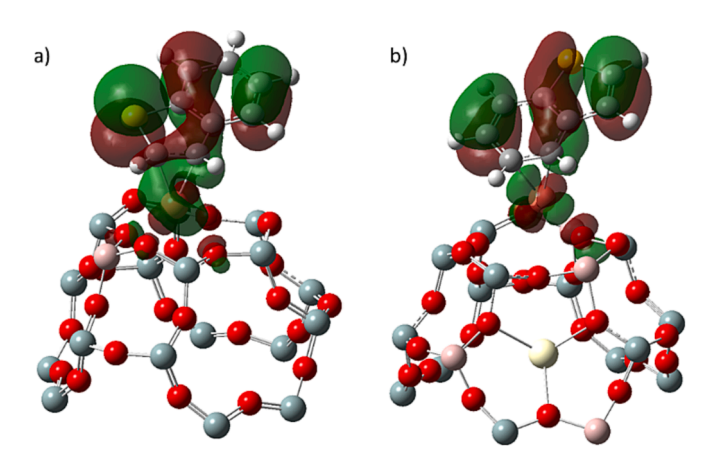


Fig. 9. BD NBOs between adsorbed BT and Cu on CuY (a) and CuCeY (b).

Table 9Selected second order perturbation stabilization energies between donor (Lewis) and acceptor (non-Lewis) orbitals for BT adsorbed on CuY and CuCeY.

Material	Spin State	Donor (L) NBO	Acceptor (NL) NBO	$\left \Delta E_{ij}^{(2)} ight $ kcal/ mol	$arepsilon_{j}^{(NL)}-arepsilon_{i}^{(L)}$ a.u.	F _{ij} a. u.
CuY-BT	closed-	LP Cu	BD* C-C	0.72	0.74	0.021
	shell	BD C-C	LV Cu	3.55	0.66	0.043
		3Cn	BD* Cu-C	302.04	0.02	0.071
		C-C-C				
CuCeY-	Alpha	LP Cu	3C* C-C-C	0.64	0.18	0.014
BT		BD C-C	LV Cu	2.33	0.52	0.044
		3Cn	BD* Cu-C	149.94	0.04	0.100
		C-C-C				
	Beta	LP Cu	3C* C-C-C	0.64	0.18	0.014
		BD C-C	LV Cu	2.33	0.52	0.044
		3Cn	BD* Cu-C	149.93	0.04	0.100
		C-C-C				

unpaired electron of Ce^{3+} giving q_i of 1 for CuCeY and 2 for CuY.

$$\Delta E_{ij}^{(2)} = -\frac{q_i |F_{ij}|^2}{\varepsilon_j^{(NL)} - \varepsilon_i^{(L)}} \tag{2}$$

The absolute values of $\Delta E_{ij}^{(2)}$ represent a net energy lowering of the NBO pair due to mixing or delocalization of orbitals. CuY and CuCeY show similar stabilizations since both follow the same adsorption mechanism for sulfur on the Cu active site. The first delocalizations involve a donor

lone pair of Cu to an acceptor π^* antibonding orbital between C atoms of the adsorbate, however with small stabilization energies of 0.72 and 0.64 kcal/mol. The second significant stabilization has a bonding C–C π orbital as a donor and an unoccupied valence orbital of Cu acceptor. These are characteristic of the π complexation adsorption mechanism that has been previously described. Overall, they show delocalization of the π resonance structure of BT to lower the energy of the overall Cu-BT adsorption system. For both CuY and CuCeY, the parameters for each stabilization are quite similar, including the stabilization energies and interaction parameters. The BD C-C to LV Cu interaction has a slightly increased stabilization energy for CuY compared to CuCeY, however the interaction parameters are similar. Another interaction between a donor three center bond of the adsorbate molecule to the acceptor BD* Cu-C has been included due to the significant stabilization energies of 302.04 kcal/mol for CuY-BT and 149.94 kcal/mol for both alpha and beta spin orbitals of CuCeY-BT. The interaction parameters are again quite similar in the CuY and CuCeY systems. This interaction shows the delocalization of the adsorbate π system electrons to the Cu cation. A complete list for of NBO stabilizations for CuY is given in Table S4 and for CuCeY in Table S5.

4. Discussion

In this study, DFT calculations were used to investigate the adsorption mechanisms of various sulfur and aromatic compounds on CuCeY. Optimization of the model zeolites found stable positions of ionexchanged Cu and Ce within the framework of Y in agreement with our earlier experimental studies. We have previously used Rietveld refinement of CuCeY X-ray diffraction (XRD) data to conclude that Ce tends to occupy the interior six-member ring sites of Y while Cu prefers sites closer to the supercage.[15] This was confirmed by in-situ XAS studies which also confirmed Cu as small particles occupying the supercage.[20] The theoretical findings in this paper found stable positions for Cu and Ce in the six-member ring sites of Y as shown in Fig. 1 and also showed Cu occupying site II in the supercage as shown in Fig. 8. Following this optimization, NBOs were calculated to determine the oxidation states of ion-exchanged metals in both bimetallic and monometallic Cu and Ce Y zeolites. The results as shown in Table 1 confirmed the presence of Cu⁺ in CuY and CuCeY, and Ce with a natural charge close to 2 e in CeY and CuCeY. However, Ce is unstable in a + 2 oxidation state, and our previous experimental work using X-ray photoelectrons spectroscopy (XPS) found Ce in the + 3 and + 4 states after ion-exchange and calcination of CuCeY.[18] In addition, in-situ XAS showed reduction of Ce^{4+} to Ce^{3+} when CuCeY was heated in the presence of H_2 . [20] Based on these previous findings we can determine that the computed 2 e natural charge from the NBOs of CuCeY is not equivalent to the oxidation state, but reflects the sharing of electrons with Ce from the framework atoms, resulting in a decreased charge. This was shown through the 2nd order stabilizations computed between donor framework NBOs and acceptor Ce LV NBOs. In CuCeY, a calculated NBO demonstrates electron sharing between Cu and Ce, as shown in Table 2. This bonding NBO with occupancy of 1 electron has the majority contribution coming from the Cu 3d orbital to the 5d and 4f orbitals of Ce. This electronic interaction between Cu and Ce is a significant difference between the bimetallic CuCeY and monometallic CuY and CeY that may play a role in the improved adsorption of sulfur on CuCeY.

With the introduction of sulfur compounds into the CuCeY zeolite supercage and subsequent optimization of the model, both direct S-M interaction and $\pi\text{-complexation}$ were found as possible adsorption modes. This confirms our previous findings using in situ diffuse reflectance infrared Fourier transform spectroscopy (DRIFTS), which suggested the presence of both adsorption mechanisms, but with $\pi\text{-complexation}$ dominating.[15] This agrees with the theoretical ΔH_{ads} calculated in this paper in Table 3, where the magnitude of ΔH_{ads} increases by 57 kJ/mol from S-M bonding to $\pi\text{-complexation}$.

Adsorption calculations of various adsorbates and Y zeolite models found theoretical ΔH_{ads} values in agreement with our previous experimental breakthrough curves, with the greatest adsorption strength and best desulfurization performance found with CuCeY. [14,18,22] However, the results in Table 4 show limited improvement in selectivity for sulfur compounds over similar competing aromatics. Therefore, the improved desulfurization of CuCeY must be due to increased adsorption capacity and stronger chemisorption rather than higher S selectivity. This is further supported by findings in Fig. 8 and Table 5 where the distortion of the Cu active site further into the supercage of CuCeY is evident, and our previous XAS experimental studies. [20].

To further study the $\pi\text{-}complexation}$ adsorption mechanism, CuCeY-BT and CuY-BT NBOs show the electronic interaction between Cu and BT with and without the presence of Ce. From Table 7 and Table 8, in both CuY and CuCeY the bonding between Cu and the π electrons of the BT aromatic ring is similar. With both models there is a 2 electron occupied bonding orbital and 1 electron antibonding orbital compromised primarily from sharing of the Cu 3d orbitals and the C 2p. This is further supported by the 2nd order stabilizations that show delocalization of BT electron density towards Cu with adsorption.

5. Conclusion

This computational study of sulfur adsorption on metal ionexchanged zeolites using DFT methods has revealed the mechanism behind the improved adsorption exhibited by CuCeY. Calculated ΔH_{ads} values are in agreement with experimental findings following CuCeY > CuY > CeY > parent Y. However, metal ion-exchanged Y models show similar affinity for S containing molecules and pure aromatics, indicating that increased adsorption can be attributed to greater capacity and stronger chemisorption rather than selectivity for sulfur. This suggests an increase in the number of available adsorption sites with the introduction of metals into Y, in agreement with previous XAS experiments. In addition, NBO calculations uncovered the synergy behind Cu and Ce cations in bimetallic Y. BD and BD* NBO pairs show sharing of electron density between Cu and Ce prior to adsorption. With sulfur adsorption the NBOs show bonding between Cu and adsorbate largely due to sharing of Cu 3d orbitals. Furthermore, significant delocalization of the sulfur compound's electron structure towards Cu is evident from the 2nd order perturbation energies. Overall, these DFT simulations have led to a better understanding of sulfur adsorption on Cu and Ce exchanged Y materials and the resulting alterations to the electronic structure. From these results, the synergy between Cu and Ce cations is better understood in regards to improving ADS performance.

CRediT authorship contribution statement

Henry J. Sokol: Data curation, Formal Analysis, Investigation,

Methodology, Writing-original draft. **Kevin X. Lee:** Investigation. **Julia A. Valla:** Conceptualization, Project administrations, Funding acquisition, resources, supervision, Writing review and editing.

Declaration of Competing Interest

The authors declare that they have no known competing financial interests or personal relationships that could have appeared to influence the work reported in this paper.

Data availability

Data will be made available on request.

Acknowledgements

We would like to acknowledge and thank Stavros Caratzoulas for his support with this computational study.

The research was funded in part by the NSF CAREER Award #1844767 and Advanced Manufacturing for Energy Systems (AMES) fellowship at the University of Connecticut, funded by US Department of Energy Advanced Manufacturing Office traineeship program, Grant No. DE-EE0008302.

Data availability

The raw data required to reproduce these findings are available to download from https://data.mendeley.com/datasets/xb4gwww68s/1. The processed data required to reproduce these findings are available to download from https://data.mendeley.com/datasets/xb4gwww68s/1.

Appendix A. Supplementary data

Supplementary Material. Figure S1: Models of HY, NaY, CuY, and CeY; Table S1: Electronic configuration of CuCeY with 5 framework Al; Table S2: 2nd order stabilization between Ce and framework atoms; Table S3: 2nd order stabilization between Cu and Ce; Figure S2: Adsorption geometries of benzene and naphthalene on CuCeY; Figure S3: Adsorption geometries on HY; Figure S4: Adsorption geometries on NaY; Figure S5: Adsorption geometries on CuY; Figure S6: Adsorption geometries on CuY; Table S4: 2nd order stabilization between Cu in CuY and BT; Table S5: 2nd order stabilization between Cu in CuCeY and BT; Table S6: Computed Enthalpies in Hartree/particle of zeolite models, adsorbates, and adsorbates on each zeolite. Supplementary data to this article can be found online at https://doi.org/10.10 16/j.commatsci.2024.112813.

References

- Q. Shi, J. Wu, Review on sulfur compounds in petroleum and its products: state-ofthe-art and perspectives, Energy Fuels 35 (2021) 14445–14461, https://doi.org/ 10.1021/acs.energyfuels.1c02229.
- [2] J.A. Valla, E. Mouriki, A.A. Lappas, I.A. Vasalos, The effect of heavy aromatic sulfur compounds on sulfur in cracked naphtha, Catal. Today. 127 (2007) 92–98, https:// doi.org/10.1016/j.cattod.2007.05.017.
- [3] S. Jafarinejad, Control and treatment of sulfur compounds specially sulfur oxides (SOx) emissions from the petroleum industry: A review, Chem. Int. 2 (2016) 242–253, https://doi.org/10.31221/osf.io/bxmsr.
- [4] R. Detels, D.P. Tashkin, J.W. Sayre, S.N. Rokaw, F.J. Massey, A.H. Coulson, D. H. Wegman, The UCLA population studies of CORD: X. A cohort study of changes in respiratory function associated with chronic exposure to SO(X), NO(X), and hydrocarbons, Am. J. Public Health. 81 (1991) 350–359, https://doi.org/10.2105/AJPH.81.3.350.
- [5] Control of Air Pollution From Motor Vehicles: Tier 3 Motor Vehicle Emission and Fuel Standards, Washington, DC, 2014.
- [6] Control of Air Pollution from New Motor Vehicles: Heavy-Duty Engine and Vehicle Standards and Highway Diesel Sulfur Control Requirements, Washington, DC, 2001.
- [7] Z. Cheng, S. Zha, M. Liu, Influence of cell voltage and current on sulfur poisoning behavior of solid oxide fuel cells, J. Power Sources. 172 (2007) 688–693, https:// doi.org/10.1016/j.jpowsour.2007.07.052.

- [8] K.X. Lee, J.A. Valla, Adsorptive desulfurization of liquid hydrocarbons using zeolite-based sorbents: A comprehensive review, React Chem. Eng. 4 (2019) 1357–1386, https://doi.org/10.1039/c9re00036d.
- [9] C. Song, An overview of new approaches to deep desulfurization for ultra-clean gasoline, diesel fuel and jet fuel, Catal. Today. 86 (2003) 211–263, https://doi.org/ 10.1016/S0920-5861(03)00412-7.
- [10] B. Saha, S. Vedachalam, A.K. Dalai, Review on recent advances in adsorptive desulfurization, Fuel Process. Technol. 214 (2021) 106685, https://doi.org/ 10.1016/j.fuproc.2020.106685.
- [11] N. Taufiqurrahmi, A.R. Mohamed, S. Bhatia, Nanocrystalline zeolite Y: Synthesis and characterization, IOP Conf. Ser. Mater. Sci. Eng. 17 (2011), https://doi.org/ 10.1088/1757-899X/17/1/012030.
- [12] Z. Qin, K.A. Cychosz, G. Melinte, H. El Siblani, J.P. Gilson, M. Thommes, C. Fernandez, S. Mintova, O. Ersen, V. Valtchev, Opening the Cages of Faujasite-Type Zeolite, J. Am. Chem. Soc. 139 (2017) 17273–17276, https://doi.org/ 10.1021/jacs.7b10316
- [13] J.W. Ward, The Nature of Active Sites on Zeolites I. The Decationated Y Zeolite, J. Catal. 9 (1967) 225–236. http://www.ncbi.nlm.nih.gov/pubmed/8822346.
- [14] K.X. Lee, J.A. Valla, Investigation of metal-exchanged mesoporous Y zeolites for the adsorptive desulfurization of liquid fuels, Appl. Catal. B Environ. 201 (2017) 359–369, https://doi.org/10.1016/j.apcatb.2016.08.018.
- [15] K.X. Lee, T.B. Crowl, H.J. Sokol, M.D. Morales-acosta, J.A. Valla, Understanding the Role of Rare Earths in Zeolite Y on the Removal of Sulfur from Hydrocarbon Fuels, J. Phys. Chem. C. 125 (2021) 9107–9118, https://doi.org/10.1021/acs. jpcc.1c01103.
- [16] Y. Zu, Z. Guo, J. Zheng, Y. Hui, S. Wang, Y. Qin, L. Zhang, H. Liu, X. Gao, L. Song, Investigation of Cu(I)-Y zeolites with different Cu/Al ratios towards the ultra-deep adsorption desulfurization: Discrimination and role of the specific adsorption active sites, Chem. Eng. J. 380 (2020) 122319, https://doi.org/10.1016/j. cei.2019.122319.
- [17] H. Song, Y. Chang, H. Song, Deep adsorptive desulfurization over Cu, Ce bimetal ion-exchanged Y-typed molecule sieve, Adsorption. 22 (2016) 139–150, https:// doi.org/10.1007/s10450-015-9731-3.
- [18] K.X. Lee, H. Wang, S. Karakalos, G. Tsilomelekis, J.A. Valla, Adsorptive Desulfurization of 4,6-Dimethyldibenzothiophene on Bimetallic Mesoporous y Zeolites: Effects of Cu and Ce Composition and Configuration, Ind. Eng. Chem. Res. 58 (2019) 18301–18312, https://doi.org/10.1021/acs.iecr.9b02346.
- [19] H. Song, H. Song, X. Wan, M. Dai, J. Zhang, F. Li, Deep desulfurization of model gasoline by selective adsorption over Cu-Ce bimetal ion-exchanged y zeolite, Fuel Process. Technol. 116 (2013) 52–62, https://doi.org/10.1016/j. fupres. 2013.04.017
- [20] H.J. Sokol, A.M. Ebrahim, S. Caratzoulas, A.I. Frenkel, J.A. Valla, In Situ XAFS, XRD, and DFT Characterization of the Sulfur Adsorption Sites on Cu and Ce Exchanged y Zeolites, J. Phys. Chem. C. 126 (2022) 1496–1512, https://doi.org/ 10.1021/acs.jpc.1c09128.
- [21] J.H. Shan, X.Q. Liu, L.B. Sun, R. Cui, Cu-Ce bimetal ion-exchanged Y zeolites for selective adsorption of thiophenic sulfur, Energy Fuels 22 (2008) 3955–3959, https://doi.org/10.1021/ef800296n.
- [22] K.X. Lee, G. Tsilomelekis, J.A. Valla, Removal of benzothiophene and dibenzothiophene from hydrocarbon fuels using CuCe mesoporous Y zeolites in the presence of aromatics, Appl. Catal. B Environ. 234 (2018) 130–142, https://doi. org/10.1016/j.apcatb.2018.04.022.
- [23] A. Botana-de la Cruz, P.E. Boahene, S. Vedachalam, A.K. Dalai, J. Adjaye, Mesoporous adsorbents for desulfurization of model diesel fuel: optimization, kinetic, and thermodynamic studies, Fuels. 1 (2020) 47–58, https://doi.org/ 10.3390/fuels1010005.
- [24] M.L.M. Navarro Cerutti, F.V. Hackbarth, D. Maass, S.S.X. Chiaro, R.R.C. Pinto, M.J. B. Cardoso, P.A. Arroyo, A.A. Ulson de Souza, S.M.A.G.U. de Souza, Copper-exchanged Y zeolites for gasoline deep-desulfurization, Adsorption. 25 (2019) 1595–1609, https://doi.org/10.1007/s10450-019-00153-y.
- [25] Y. Wang, F.H. Yang, R.T. Yang, J.M. Heinzel, A.D. Nickens, Desulfurization of highsulfur jet fuel by π-complexation with copper and palladium halide sorbents, Ind. Eng. Chem. Res. 45 (2006) 7649–7655, https://doi.org/10.1021/ie060922w.
- [26] A.J. Hernández-Maldonado, R.T. Yang, Desulfurization of Diesel Fuels by Adsorption via π-Complexation with Vapor-Phase Exchanged Cu(I)-Y Zeolites, J. Am. Chem. Soc. 126 (2004) 992–993, https://doi.org/10.1021/ja039304m.
- [27] X.L. Song, L.B. Sun, G.S. He, X.Q. Liu, Isolated Cu(I) sites supported on β-cyclodextrin: An efficient π-complexation adsorbent for thiophene capture, Chem. Commun. 47 (2011) 650–652, https://doi.org/10.1039/c0cc04587j.
- [28] A.J. Hernández-Maldonado, R.T. Yang, New Sorbents for Desulfurization of Diesel Fuels via π-Complexation, AIChE J. 50 (2004) 791–801, https://doi.org/10.1002/ aic.10074
- [29] Z. Mo, Y. Qin, Y. Zu, H. Wang, X. Zhang, L. Song, Effect of Content of Cerium Ion on Brönsted-Acid-Catalyzed Reaction of Thiophene over CeY Zeolite Studied by In Situ FTIR Spectroscopy, ChemistrySelect. 4 (2019) 13034–13044, https://doi.org/ 10.1002/slct.201903194.
- [30] X. Gao, W. Geng, H. Zhang, X. Zhao, X. Yao, Thiophenic compounds adsorption on Na(I)Y and rare earth exchanged y zeolites: A density functional theory study,

- J. Mol. Model. 19 (2013) 4789–4795, https://doi.org/10.1007/s00894-013-1954-
- [31] L. Wang, Z. Sun, Y. Ding, Y. Chen, Q. Li, M. Xu, H. Li, L. Song, A theoretical study of thiophenic compounds adsorption on cation-exchanged y zeolites, Appl. Surf. Sci. 257 (2011) 7539–7544, https://doi.org/10.1016/j.apsusc.2011.03.115.
- [32] J. Jiang, F.T.T. Ng, Production of low sulfur diesel fuel via adsorption: An equilibrium and kinetic study on the adsorption of dibenzothiophene onto NaY zeolite, Adsorption. 16 (2010) 549–558, https://doi.org/10.1007/s10450-010-9250-5
- [33] H. Song, Y. Chang, X. Wan, M. Dai, H. Song, Z. Jin, Equilibrium, kinetic, and thermodynamic studies on adsorptive desulfurization onto CuICeIVY zeolite, Ind. Eng. Chem. Res. 53 (2014) 5701–5708, https://doi.org/10.1021/ie403177t.
- [34] E.P. Hessou, H. Jabraoui, I. Khalil, M.A. Dziurla, M. Badawi, Ab initio screening of zeolite Y formulations for efficient adsorption of thiophene in presence of benzene, Appl. Surf. Sci. 541 (2021) 148515, https://doi.org/10.1016/j. apsusc. 2020 148515
- [35] J. Fujiki, E. Furuya, Density functional theory study of adsorption of benzothiophene and naphthalene on silica gel, Fuel. 164 (2016) 180–185, https://doi.org/10.1016/i.fuel.2015.10.013.
- [36] C.Y. Sung, S. Al Hashimi, A. McCormick, M. Cococcioni, M. Tsapatsis, A DFT study on multivalent cation-exchanged y zeolites as potential selective adsorbent for H2S, Microporous Mesoporous Mater. 172 (2013) 7–12, https://doi.org/10.1016/ i.micromeso.2012.12.006.
- [37] H. et al. Frisch, M. J. Trucks, G. W. Schlegel, H. B. Scuseria, G. E. Robb, M. A. Cheeseman, J. R. Scalmani, G. Barone, V. Petersson, G. A. Nakatsuji, Gaussian 16, (2016)
- [38] T. Archipov, S. Santra, A.B. Ene, H. Stoll, G. Rauhut, E. Roduner, Adsorption of Benzene to Copper in CuHY zeolite, J. Phys. Chem. C. 113 (2009) 4107–4116.
- [39] S. Santra, T. Archipov, A.B. Ene, H. Komnik, H. Stoll, E. Roduner, G. Rauhut, Adsorption of dioxygen to copper in CuHY zeolite, Phys. Chem. Chem. Phys. 11 (2009) 8855–8866, https://doi.org/10.1039/b904152d.
- [40] A.D. Becke, A new mixing of Hartree-Fock and local density-functional theories, J. Chem. Phys. 98 (1993) 1372–1377, https://doi.org/10.1063/1.464304.
- [41] C. Lee, W. Yang, R.G. Parr, Developement of the Colle-Salvetti Correlation-Energy Formula into a Functional of the Electron Density, Phys. Rev. B. 37 (1988) 785–789
- [42] V.A. Rassolov, J.A. Pople, M.A. Ratner, T.L. Windus, 6–31G* basis set for atoms K through Zn, J. Chem. Phys. 109 (1998) 1223–1229, https://doi.org/10.1063/ 1.476673.
- [43] P.C. Hariharan, J.A. Pople, The influence of polarization function on molecular orbital hydrogenation energies, Theor. Chim. Acta. 28 (1973).
- [44] W.J. Hehre, R. Ditchfield, J.A. Pople, Self Consistent Molecular Orbital Methods. XII. Further Extensions of Gaussian — Type Basis Sets for Use in Molecular Orbital Studies of Organic Molecules, J. Chem. Phys. 56 (1972) 2257–2261.
- [45] M.M. Francl, W.J. Pietro, W.J. Hehre, J.S. Binkley, M.S. Gordon, D.J. DeFrees, J. A. Pople, Self-consistent molecular orbital methods. XXIII. A polarization-type basis set for second-row elements, J. Chem. Phys. 77 (1982) 3654–3665, https://doi.org/10.1063/1.444267.
- [46] S. Gordon, J.S. Binkley, J.A. Pople, W.J. Pietro, W.J. Hehre, Self-Consistent Molecular-Orbital Methods. 22. Split-Valence Basis Sets for Second-Row Elements, J. Am. Chem. Soc. 104 (1982) 2797–2803.
- [47] A.K. Rappé, C.J. Casewit, K.S. Colwell, W.A. Goddard, W.M. Skiff, UFF, a Full Periodic Table Force Field for Molecular Mechanics and Molecular Dynamics Simulations, J. Am. Chem. Soc. 114 (1992) 10024–10035, https://doi.org/ 10.1021/ja00051a040.
- [48] M. Dolg, H. Preuss, Energy-adjusted ab initio pseudopotentials for the rare earth elements, J. Chem. Phys. 90 (1989) 1730–1734.
- [49] B.P. Pritchard, D. Altarawy, B. Didier, T.D. Gibson, T.L. Windus, New Basis Set Exchange: An Open, Up-to-Date Resource for the Molecular Sciences Community, J. Chem. Inf. Model. 59 (2019) 4814–4820, https://doi.org/10.1021/acs. icim.9b00725.
- [50] M. Ravi, V.L. Sushkevich, J.A. van Bokhoven, Towards a better understanding of Lewis acidic aluminium in zeolites, Nat. Mater. 19 (2020) 1047–1056, https://doi. org/10.1038/s41563-020-0751-3.
- [51] W. Loewenstein, The distribution of aluminum in the tetrahedra of silicates and aluminates, Am. Mineral. 39 (1954) 92–96.
- [52] D. Berthomieu, S. Krishnamurty, B. Coq, G. Delahay, A. Goursot, Theoretical modeling of a copper site in a Cu(II) - Y zeolite, J. Phys. Chem. B. 105 (2001) 1149–1156, https://doi.org/10.1021/jp002929b.
- [53] W.W. Lukens, M. Speldrich, P. Yang, T.J. Duignan, J. Autschbach, P. Kögerler, The roles of 4f- and 5f-orbitals in bonding: A magnetochemical, crystal field, density functional theory, and multi-reference wavefunction study, Dalt. Trans. 45 (2016) 11508–11521, https://doi.org/10.1039/c6dt00634e.
- [54] C. Sun, K. Li, D. Xue, Searching for novel materials via 4f chemistry, J. Rare Earths. 37 (2019) 1–10, https://doi.org/10.1016/j.jre.2018.06.002.
- [55] Y. Shi, X. Yang, F. Tian, C. Jia, Y. Chen, Effects of toluene on thiophene adsorption over NaY and Ce(IV)Y zeolites, J. Nat. Gas Chem. 21 (2012) 421–425, https://doi. org/10.1016/S1003-9953(11)60385-X.